

Supporting Information

Contents

1. X-ray structure analysis – Experimental details on crystal structure analysis of compounds **1A**, **9B** and **10B** at room temperature
 2. Detailed overview of conformational properties of the crystalline cyclodipeptides
 3. The amount (in %) of Hirshfeld surface associated with close contacts between atoms X and Y in DKPs **1A - 2B** and **9A – 10B**.
 4. Cartesian coordinates of HB optimized structures
 5. Brillouin zone sampling in the periodic calculations
- 1. X-ray structure analysis – Experimental details on crystal structure analysis of compounds 1A, 9B and 10B at room temperature**

Crystal Data	1A^{room}	9B^{room}	10B^{room}
Formula	2(C ₁₅ H ₁₈ N ₄ O ₄).H ₂ O	C ₁₄ H ₁₆ N ₂ O ₂	C ₁₅ H ₁₈ N ₂ O ₂
Formula Weight	534.64	244.29	258.31
Crystal System	Orthorhombic	Monoclinic	Orthorhombic
Space group	P2 ₁ 2 ₁ 2 ₁ (No.19)	P2 ₁ (No.4)	P2 ₁ 2 ₁ 2 ₁ (No.19)
a, b, c [Å]	8.5217(1) 25.0552(3) 13.4521(2)	8.0807(7) 6.6311(6) 12.0895(9)	10.1490(5) 10.939(1) 12.310(1)
α, β, γ [deg]	90 90 90	90 96.428(7) 90	90 90 90
V [Å ³]	2872.20(6)	643.73(9)	1366.66(18)
Z	4	2	4
D(calc)[g/cm ³]	1.236	1.260	1.255
μ(MoKa) [1/mm]	0.085	0.085	0.084
F(000)	1144	260	552
Crystal Size [mm]	0.30 x 0.40 x 0.40	0.10 x 0.30 x 0.60	0.30 x 0.40 x 0.50
Data Collection			
Temperature (K)	297	293	293
T _{max} [Deg]	26.0	25.0	25.0
Dataset	-10: 10; -30: 30; -16: 16	-9: 9; -7: 7; 0: 14	0: 12; 0: 12; 0: 14
Tot., Uniq. Data, R(int) ^a	50418, 5656, 0.032	2263, 2212, 0.028	1386, 1386
Observed data [I > 2.0 σ(I)]	4670	1942	1179
Refinement			
Nref, Npar	5656, 368	2212, 167	1386, 174
^b R[F ² > 2σ(F ²)]	0.0347	0.0399	0.0346
wR(F ²), S(all data)	0.0931, 1.04	0.1077, 1.05	0.1011, 1.07
Flack x	0.0(8)	-0.2(15)	-3(2)
? ? _{min} , ? ? _{max}	-0.12, 0.09	-0.22, 0.19	-0.17, 0.13

$$^a R_{\text{int}} = \frac{\sum |F_o^2 - F_{o,\text{mean}}^2|}{\sum F_o^2}; ^b R(F) = \frac{\sum ||F_o| - |F_c||}{\sum |F_o|}; wR(F^2) = \frac{[\sum(w(F_o^2 - F_c^2)^2)/(\sum w(F_o^2)^2)]^{1/2}}{[\sum(w(F_o^2 - F_c^2)^2)/(N_{\text{diffs}} - N_{\text{params}})]^{1/2}}. S =$$

2. Detailed overview of conformational properties of the crystalline cyclodipeptides
 Conformation of DKP-ring, annealed Pip or Pro ring and orientation of Phe ring in the considered series of cyclodipeptides (from X-ray data at 150 K).

No. Compound	DKP ring		Pip and/or Pro	Phe-ring
	Ring conformation	Nonplanarity of peptide bonds	Chair-form contribution [mol. fraction]	Orientation (angle α)
1A c(L-Pip-L-Phe)	family of 4 molecules: $l = +5.3$ to $+12.4$; $t = -1.0$ to $+5.1$ ${}^C T^{C\alpha} \leftrightarrow {}^{C\alpha} B$	slightly nonplanar: $\omega_1 = -4.9$ to $+0.5$ $\omega_2 = -0.6$ to $+8.1$	$X_C = 0.15$ to 0.42	γC^N F (62 to 67)
1B c(L-Pip-D-Phe)	family of 6 molecules: $l = -6.5$ to $+4.0$; $t = -1.1$ to $+3.2$ ${}^{C\alpha} T^N$ (flattened)	strongly nonplanar: $\omega_1 = +15.6$ to $+17.8$ $\omega_2 = -14.1$ to -5.9	$X_C = 0.62$ to 0.93	γC^N F (57 to 66)*
2A c(L-Pip-L-(NMe)Phe)	2 molecules $l \approx +16$; $t \approx -12$ ${}^N B \leftrightarrow {}^{C\alpha} T^N$	strongly nonplanar: $\omega_1 \approx -17$ $\omega_2 \approx -10$	$X_C \approx 0.15$	γC^N F (≈ 66)
2B c(D-Pip-L-(NMe)Phe)	$l = -20.0^*$; $t = +4.1^*$ ${}^{C\alpha} T^N$	medium nonplanar: $\omega_1 = +10.7^*$ $\omega_2 = +3.2^*$	$X_C = 0.16$	γC^N F (68)
9A c(L-Pro-L-Phe)	$l = -53.7$; $t = -8.9$ ${}^{C\alpha} B$	slightly nonplanar: $\omega_1 = -0.8$ $\omega_2 = -4.2$	$X_C = 0.03$	$P = 4.8$ (${}^{\gamma} T_{\beta}$) $\tau_m = 37.6$ E_N (-80)
9B c(L-Pro-D-Phe)	$l = -18.3$; $t = -1.7$ ${}^{C\alpha} B$ (flattened compared to 9A)	nearly planar: $\omega_1 = +0.3$ $\omega_2 = +0.3$	$X_C = 0.03$	$P = -29.8$ (${}^{\alpha} T_{\beta}$) $\tau_m = 39.9$ F (78)*
10A c(L-Pro-L-(NMe)Phe)	$l = +9.2$; $t = -8.2$ ${}^N B \leftrightarrow {}^{C\alpha} T^N$	strongly nonplanar: $\omega_1 = -17.9$ $\omega_2 = -1.4$	$X_C = 0.42$	$P = -53.1$ (${}^{\alpha} E$) $\tau_m = 38.4$ F (65)
10B c(L-Pro-D-(NMe)Phe)	$l = -31.0$; $t = -1.8$ ${}^{C\alpha} B$	nearly planar: $\omega_1 = +1.8$ $\omega_2 = +1.4$	$X_C = 0.01$	$P = -17.1$ (${}^{\beta} E$) $\tau_m = 41.4$ F (68)*

* The signs of these parameters for D-residue were changed to be comparable with those for L-residues.

3. The amount (in %) of Hirshfeld surface associated with close contacts between atoms X and Y in DKPs 1A - 2B and 9A – 10B. Multiple conformers are distinguished by label m1, ... m6.

X ... Y	1A m1	1A m2	1A m3	1A m4	1B m1	1B m2	1B m3	1B m4	1B m5	1B m6
N ... N	0	0	0	0	0	0	0	0	0	0
N ... C	0.1	0	0	0.2	0	0	0	0	0	0
N ... H	0.4	1.3	1.3	0.7	0.8	0.4	0.5	0.5	0.8	0.6
N ... O	0.5	0.3	0.1	0.5	0	0	0	0	0	0
C ... N	0	0.2	0.1	0	0	0	0	0	0	0
C ... C	0.1	0.2	0.1	0.2	0	0.2	0.1	0.3	0.3	0.1
C ... H	5.6	5.7	5.9	5.6	6.4	5.6	6.2	5.5	5.5	6.1
C ... O	0.4	0.3	0.4	0.4	0	0	0	0	0	0
H ... N	1.1	0.3	0.2	1.2	0.4	0.5	0.2	0	0.8	0.6
H ... C	3.5	3.4	3.0	4.4	4.4	4.4	4.7	4.6	4.4	4.3
H ... H	66.6	67.0	66.9	65.6	67.0	69.2	67.5	68.4	67.7	67.7
H ... O	10.5	9.5	10.3	10.0	9.7	9.2	9.8	10.0	9.9	9.5
O ... N	0.1	0.5	0.5	0.2	0	0	0	0	0	0
O ... C	0.2	0.3	0.4	0.2	0	0	0	0	0	0
O ... H	10.9	11.0	10.8	10.8	11.2	10.5	11.0	10.7	10.5	11.0
O ... O	0	0	0	0	0	0	0	0	0	0

X ... Y	2A m1	2A m2	2B	9A	9B	10A	10B
N ... N	0	0	0	0	0	0.7	0
N ... C	0	0	0	0	0	0	0
N ... H	1.6	1.6	1.0	1.2	0.9	1.0	0.9
N ... O	0	0	0	0.1	0	0	0
C ... N	0	0	0	0	0	0	0
C ... C	0	0	0	0.4	0.3	0.1	0
C ... H	5.6	5.7	5.8	9.9	6.9	6.3	6.4
C ... O	0.4	0.4	0.3	0.8	0	0	0.3
H ... N	1.6	1.6	1.0	1.1	0.9	1.0	0.9
H ... C	4.6	4.3	4.6	6.7	5.0	5.8	4.8
H ... H	67.6	67.9	68.4	57.5	64.0	66.4	65.7
H ... O	8.5	8.4	9.1	9.8	10.0	9.8	9.7
O ... N	0	0	0	0.1	0	0	0
O ... C	0.2	0.3	0.1	0.8	0	0	0.1
O ... H	9.9	9.8	9.7	11.3	12.0	8.8	11.3
O ... O	0	0	0	0.1	0	0	0

5. Brillouin zone sampling in the periodic calculations

In order to accurately mimic the crystal state of the DKPs, it is imperative to take into account the full molecular environment of each molecule, which can be achieved by applying periodic boundary conditions. Using this approach, geometry optimizations were first performed, using the unit cell structures that were determined from X-ray diffraction as a starting point. Ideally, these optimizations would not involve any changes to the initial structures. However, since all computational methods are essentially approximate, this is not the case. Therefore, such calculations first of all indicate how accurate the adopted approach is in treating the intra- and intermolecular interactions that govern the crystal.

For most of the compounds, all calculated structural parameters remained quite close to those of the crystal structures. However, significant changes were apparent in **1B** and **9B**. The puckering of both cyclic dipeptide rings proved fundamentally incorrect, although the aliphatic ring substituents (Pip or Pro) were less affected. The origin of this failure in the computational procedure was traced by reoptimizing a benchmark compound **9B** with various modifications to the optimization method. In Table SI-1, the calculated endocyclic dihedral angles of the dipeptide are compared with the values in the crystal. The structural parameters in the first column were obtained by optimizing the unit cell using Vanderbilt (Vdb) pseudopotentials at a 25 Ry cutoff with a BP86 functional, as described in the computational details. Reoptimization of the unit cell with a BLYP functionalⁱ, Troullier-Martins type (MT) pseudopotentialsⁱⁱ or a higher cutoff of the plane wave basis set (columns 2-5) yielded essentially similar (incorrect) puckering parameters for **9B**. So, the used density functional, pseudopotential type or basis set expansion were clearly not the cause of the discrepancy.

Table SI-1 DKP ring torsion angles (in degrees) in compound **9B** as obtained from various periodic optimization schemes. For each calculation is indicated: size of periodic cell, type of pseudopotential, density functional, wave function cutoff, and size of k -point mesh. For reference, the crystal data is given.

Torsion angle	Crystal	(1)	(2)	(3)	(4)	(5)
		Unit cell				
		Vdb	Vdb	Vdb	MT	MT
		BP86	BLYP	BP86	BP86	BLYP
		25 Ry	25 Ry	100 Ry	70 Ry	70 Ry
		Γ only	Γ only	Γ only	Γ only	Γ only
ϕ 1	-17.2	3.4	3.7	2.7	1.9	2.5
ψ 1	15.0	-4.6	-4.8	-4.1	-3.4	-4.4
ω 1	2.9	18.5	18.4	18.3	17.5	19.1
ϕ 2	-19.2	-28.2	-27.6	-28.2	-27.2	-29.0
ψ 2	16.6	24.0	23.6	23.9	22.9	24.1
ω 2	0.8	-13.8	-13.9	-13.2	-12.3	-13.2

Torsion angle	Crystal	(6)	(7)	(8)	(9)	(10)	(11)	
		Unit cell				<a2bc> supercell		
		MT	MT	MT	MT	Vdb	MT	
		BLYP	BLYP	BLYP	BLYP	BP86	BLYP	
70 Ry	70 Ry	70 Ry	70 Ry	25 Ry	70 Ry			
		2x1x1	1x2x1	1x1x2	5x5x5	Γ only	Γ only	
ϕ_1	-17.2	3.6	-16.3	2.6	-16.2	-14.7	-16.1	
ψ_1	15.0	-3.9	14.9	-4.0	14.5	13.1	13.7	
ω_1	2.9	16.8	2.6	18.4	3.2	4.3	4.5	
ϕ_2	-19.2	-26.4	-19.1	-28.2	-19.5	-20.2	-20.7	
ψ_2	16.6	23.3	17.3	23.8	17.4	17.9	17.7	
ω_2	0.8	-14.1	-0.4	-13.3	-0.4	-1.4	-0.3	

Instead, it appears that the way in which the Brillouin zone integration was carried out in the periodic calculations heavily influenced the result. So far, this integral was reduced to only an evaluation at the center of the reciprocal space of the unit cell (the G-point). Yet, by sampling several k -points within the (first) Brillouin zone, a much better electronic description of the crystal was obtained. The Monkhorst-Packⁱⁱⁱ scheme – in CPMD only implemented for MT pseudopotentials – was used to construct a uniform ($M \times M \times M$) k -point mesh of increasing density ($M = 1? 5$). The total energy of the system after optimization of the unit cell clearly converges as a function of the mesh density. This is illustrated in Figure SI-1.

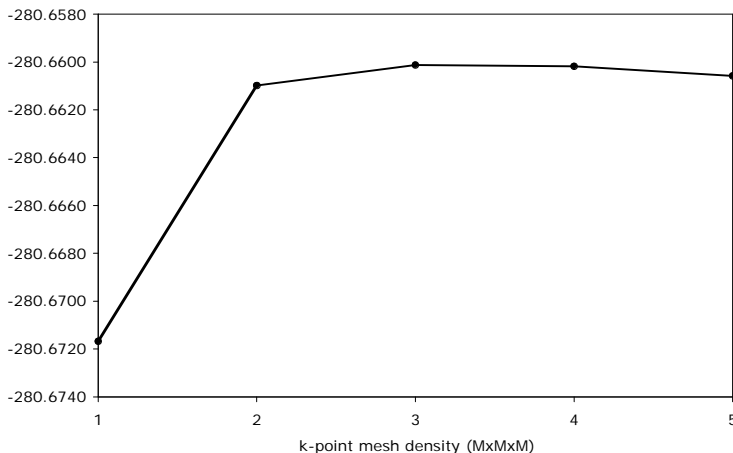


Figure SI-1 Convergence of energy as a function of k -point mesh size in a periodic unit cell optimization of **9B**.

A sharp change of the energy (~ 0.01 a.u.) is apparent between the G-only approximation and a $2 \times 2 \times 2$ k -point mesh, after which much smaller fluctuations occur (0.001 a.u. or less). The structure obtained from the geometry optimization converges in much the same fashion as a function of k -point density. In fact, it hardly changes at all when more than one k -point is considered. As an example, the result of the $5 \times 5 \times 5$ geometry optimization is taken up in Table SI-1. The calculated puckering parameters now completely agree with those of the crystal. Hence, it can be concluded that the structural discrepancies between the crystal and the initial unit cell optimizations of both **9B** and **1B** were due to the insufficient description of the k -space. Since the energy depends on the accuracy of the Brillouin zone sampling scheme, so will the atomic relaxations during geometry optimization. Within the G-only approximation, the incorrect electronic description ultimately leads to an erroneous

optimum conformation of the DKP ring. The sensitivity of the DKP ring conformation to this essentially electronic effect is quite remarkable and indicates that the band structure of the crystal is also a determining factor of the cyclodipeptide structure in the solid state.

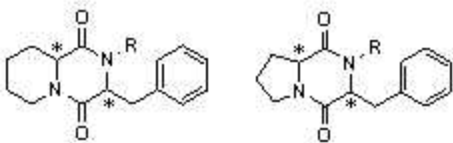
But even not as much k -points need to be included to obtain a correct crystal geometry. In Table SI-1, optimized parameters are shown for the **9B** benchmark in which only two Monkhorst-Pack generated points were taken into account. When the sampling is performed along the $\langle 1/a \rangle$ or $\langle 1/c \rangle$ reciprocal crystal directions, an incorrect geometry is again obtained. However, when the Brillouin zone is sampled along the $\langle 1/b \rangle$ direction, geometry is found which corresponds quite nicely with that of the 5x5x5 M-P mesh optimization. This reflects the size of the simulation cell. In **9B**, as well as **1B**, the $\langle b \rangle$ cell vector is only about 6 Å and much smaller than the $\langle a \rangle$ or $\langle c \rangle$ cell vectors. The Brillouin zone, therefore, is more extended along the reciprocal $\langle 1/b \rangle$ direction and the G point is hardly representative. An alternative for k -point sampling within the unit cell would then be to artificially reduce the Brillouin zone along this direction. That can be achieved by doubling the original unit cell along $\langle b \rangle$ and treating this $\langle a2bc \rangle$ supercell within a G-only approximation. Table SI-1 lists optimized puckering parameters for this computational approach. It is clear that a very reasonable description of the crystal structure is obtained, regardless of the used density functional or type of pseudopotentials. Since Vanderbilt pseudopotentials allow the plane wave basis set cutoff to be much smaller than the Troullier-Martins type, the former offer a drastic reduction of the computational cost. Hence, in view of the number of molecules in the unit cell of some of the compounds, $\langle a2bc \rangle$ supercell optimizations were performed on **1B** and **9B**, whereas an $\langle 2abc \rangle$ supercell was adopted for **1A**, **2A**, **2B** and **10B**.

-
- ⁱ A. D. Becke, *Phys. Rev. A*, 1988, **38**, 3098-3100.
C. T. Lee, W. T. Yang, R. G. Parr, *Phys. Rev. B*, 1988, **37**, 785-789.
- ⁱⁱ N. Troullier, J. L. Martins, *Phys. Rev. B*, 1991, **43**, 1993-2006.
- ⁱⁱⁱ H. J. Monkhorst, J. D. Pack, *Phys. Rev. B*, 1976, **13**, 5188-5192.

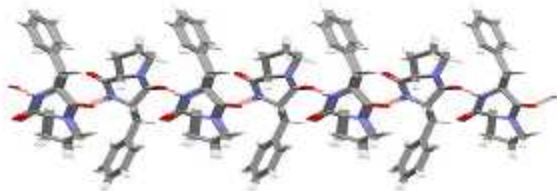
Crystal structures of cyclic dipeptides. An X-ray and computational study of *cis*- and *trans*-cyclo(Pip-Phe), cyclo(Pro-Phe) and their *N*-methyl derivatives

Milos Budesinsky, Ivana Cisarova, Jaroslav Podlaha, Frans Borremans, Jose C. Martins, Michel Waroquier, Ewald Pauwels, *Acta Crystallographica Section B*, ...

DOI:



* = LL- and LD-, R = H and CH₃



X-Ray structures of eight cyclic dipeptides are described. Advanced computer simulations of the molecules in the isolated state as well as in the crystal environment allowed separate in part intermolecular from intramolecular effects.